PROCEEDINGS OF SPIE

SPIEDigitalLibrary.org/conference-proceedings-of-spie

New technologies for the Tenerife Microwave Spectrometer and current status

Alonso-Arias, Paz, Rubiño-Martín, José Alberto, Hoyland, Roger, Aguiar-González, Marta, de-Miguel-Hernández, Javier, et al.

Paz Alonso-Arias, José Alberto Rubiño-Martín, Roger J. Hoyland, Marta Aguiar-González, Javier de-Miguel-Hernández, Ricardo T. Génova-Santos, Maria F. Gomez-Reñasco, Federica Guidi, Mateo Fernández-Torreiro, Pablo A. Fuerte-Rodríguez, Carlos Hernández-Monteagudo, Carlos H. López-Caraballo, Angeles Perez-de-Taoro, Michael W. Peel, Rafael Rebolo-López, Antonio Zamora-Jimenez, Eduardo D. González-Carretero, Carlos Colodro-Conde, Cristina Perez-Lemus, Rafael Toledo-Moreo, Francesco Cuttaia, Luca Terenzi, Cristian Franceschet, Sabrina Realini, "New technologies for the Tenerife Microwave Spectrometer and current status," Proc. SPIE 11447, Ground-based and Airborne Instrumentation for Astronomy VIII, 114476N (13 December 2020); doi: 10.1117/12.2561353

SPIE.

Event: SPIE Astronomical Telescopes + Instrumentation, 2020, Online Only

New technologies for the Tenerife Microwave Spectrometer and current status

Paz Alonso-Arias[a,b], José Alberto Rubiño-Martín[a,b], Roger J. Hoyland[a,b], Marta Aguiar-Gonzalez[a,b], Javier de-Miguel-Hernandez[a,b], Ricardo T. Genova-Santos[a,b], Maria F. Gomez-Reñasco[a,b], Federica Guidi[a,b], Mateo Fernandez-Torreiro[a,b], Pablo A. Fuerte-Rodriguez[a,b], Carlos Hernández-Monteagudo[a,b], Carlos H. López-Caraballo[a,b,j], Angeles Perez-de-Taoro[a,b], Michael W. Peel[a,b], Rafael Rebolo[a,b,i], Antonio Zamora-Jimenez[a,b], Eduardo D. González-Carretero[a,b], Carlos Colodro-Conde[a,c], Cristina Perez-Lemus[d], Rafael Toledo-Moreo[d], Francesco Cuttaia[e], Luca Terenzi[e], Cristian Franceschet[f], and Sabrina Realini[f]

[a]Instituto de Astrofísica de Canarias, Calle Vía Láctea SN, ES38205 La Laguna, Spain
[b]Departamento de Astrofísica Universidad de La Laguna, ES38205, La Laguna, Spain
[c]IAC Technology, Parque Científico y Tecnológico de Tenerife S.A. Calle Rectora María Luisa Tejedor Salguero. Parque Urbano Las Mantecas, Edificio Nanotec, 38320 San Cristóbal de La Laguna, Spain
[d]Escuela Técnica Superior de Ingeniería de Telecomunicación, Universidad Politécnica de Cartagena, Edif. Antigones, Cartagena, 30202, Spain
[e]Istituto Nazionale di Astrofisica, via Gobetti 93/3, 40129 Bologna - Italy
[f]Università degli Studi di Milano, Via Festa del Perdono 7 - 20122 Milano, Italy

ABSTRACT

The Tenerife Microwave Spectrometer (TMS) is part of a renewed effort to study and characterize the CMB frequency distribution. The spectrometer is based on a pseudo-correlation architecture with two 10–20 GHz radiometer chains making use of both orthogonal linear polarizations, and will observe in this band with an angular and frequency resolutions of 3° and 1 MHz. The optical arrangement includes two corrugated feedhorns, one facing an internal calibrator to provide a cold reference signal, and the other pointing to the sky through the cryostat window by means of an offset-fed reflector. The optical system provides optimal cross-polarization properties (≤ -30 dB) and symmetric beams, with minimum frequency dependence. The readout system is based on a SoC FPGA, providing fast data acquisition, high spectral resolution and stability. We present the current status of the TMS instrument, having described the scientific case of this instrument in the accompanying publication.

Keywords: CMB observations, ground-based experiments, radio-spectrometer, cryogenic system, ultra-wide bandwidth systems

1. INTRODUCTION

The study of the Cosmic Microwave Background (CMB) is a powerful tool used in modern Cosmology as a window to the early Universe. Many experiments have been mapping and characterizing the anisotropies and polarization patterns in the CMB over the last decades, with increasingly higher sensitivities and angular resolutions. This is particularly the case of the latest generation of satellite-based instruments, such as WMAP[1] and Planck.[2]

In contrast, since the *COBE* FIRAS team found the CMB to present an almost perfect frequency spectrum of a blackbody at a temperature of $2.726\,\mathrm{K}\pm0.57\,\mathrm{mK}$,[3] this feature remains almost unstudied. The CMB spectrum

Further author information: (Send correspondence to A.A.A.)
A.A.A.: E-mail: pazaa@iac.es, Telephone: +34 922 605200
B.B.A.: E-mail: rjh@iac.es, Telephone: +34 922 605200

Ground-based and Airborne Instrumentation for Astronomy VIII, edited by Christopher J. Evans, Julia J. Bryant, Kentaro Motohara, Proc. of SPIE Vol. 11447, 114476N · © 2020
SPIE · CCC code: 0277-786X/20/$21 · doi: 10.1117/12.2561353

is, by itself, an independent source of information that opens a window to the thermal history of the Universe. In particular, the standard cosmological model predicts distortions throughout most of the history of the Universe, with an origin related to physical mechanisms acting both before and after the recombination epoch. These distortions are mostly expected in the lower band of the observed CMB spectrum, which was not covered by FIRAS despite its wide spectral range. Some balloon-based experiments such as TRIS,[4] ARCADE and ARCADE 2,[5] were proposed to bridge this gap. In addition to this, there is an interest in the spectral characteristics of other sky emission components such as the synchrotron radiation, in order to confirm the last results reported by the ARCADE 2 team[5] at 3–90 GHz.

In this scientific context, we propose a ground-based instrument for CMB spectral measurements between 10–20 GHz with a sensitivity of $2\,\mathrm{mK}/\sqrt{\mathrm{Hz}}$ per subband. The Tenerife Microwave Spectrometer, TMS, is a novel ultra-wide band instrument. Situated in the Izaña Observatory in Tenerife (Spain), this instrument shall provide inter-frequency cross-calibration for QUIJOTE and monitor the ozone and water vapor content to characterize the atmospheric stability above the observatory. More specific details about the scientific scope of this project are given in the accompanying article.[6] However, we underline the need for an instrument that provides high physical temperature stability for the sensitive cooled components. An absolute measurement of sky temperature can only be obtained by comparing the sky signal with a stable cryogenic pseudo-blackbody. The temperature and stability of this load must be well known. The microwave optical components are particularly critical in this design since we need almost ideal radiometric and optical performance over an octave band. There must also be a high level of control of the thermal stability throughout the cryostat and electromagnetic symmetry through each RF chain measuring sky and load signals. For this reason, we have taken great care in the design detail of all the cryogenic components and set a "best effort" goal on the final performance.

In this article, we present the technological solutions specifically developed for the TMS instrument to date, in addition to presenting its current status. In Sec. 2, we describe the general layout of the instrument and in Sec. 3, we present the TMS cryostat. Section 4 includes the opto-mechanical aspects of the TMS instrument design and a brief description of the beam characterization. We describe the RF subsystems related to the correlation scheme in Sec. 5 and the readout and data storage systems in Sec. 6. Finally, Sec. 7 summarizes the current status of the TMS, remaining work and timeline to this day.

2. THE GENERAL LAYOUT OF THE TMS INSTRUMENT

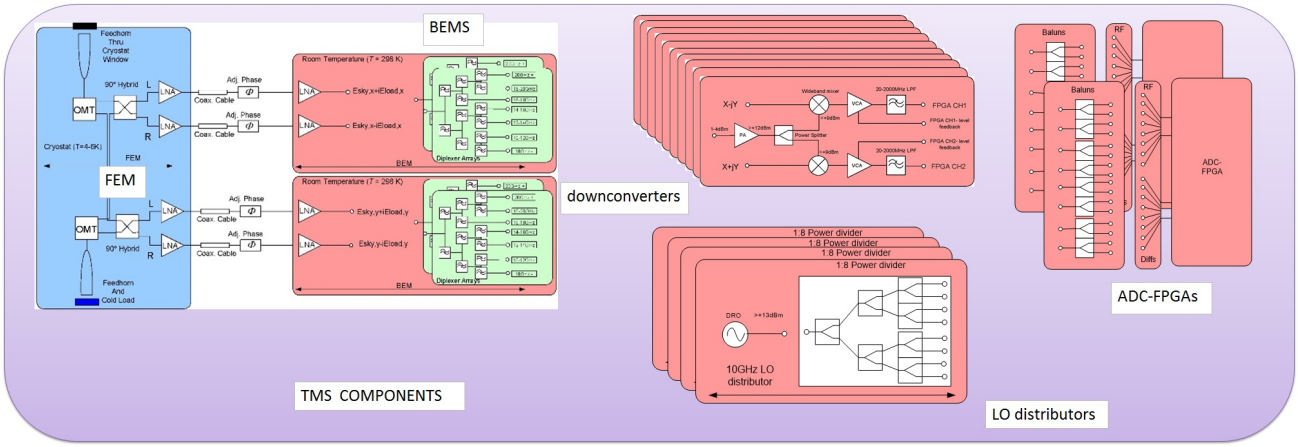

Figure 1: Schematic diagram of the general layout of the TMS instrument.

The TMS instrument is an ultra-high sensitive radio-spectrometer that consists of a cryogenically cooled front-end covering the whole band of 10–20 GHz through each of two pseudo-correlators, which are stabilized with a 4 K reference load. The radiometers are heterodyne and the band is initially divided up into 4 subbands in order to be directly acquired through ultrafast ADCs and FPGA. The data are averaged and then saved offline in a PC that is also responsible for quick-look software to monitor the system.

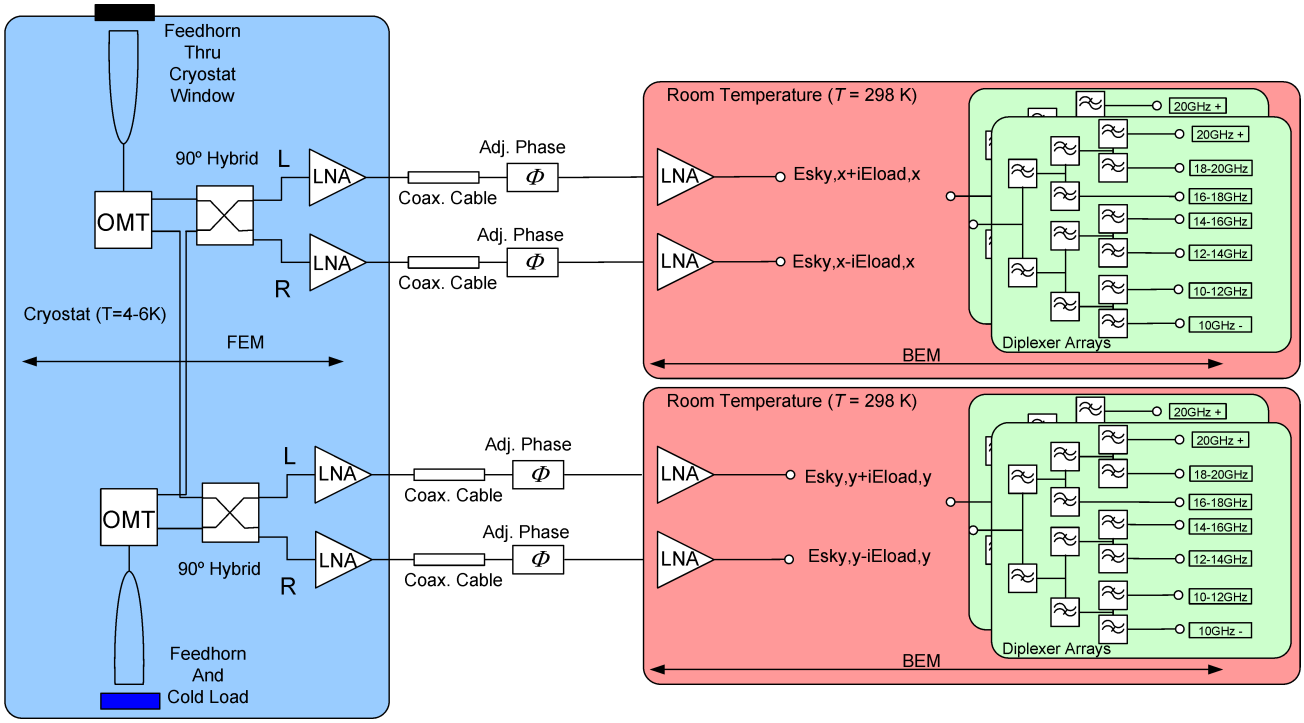

Figure 2: Schematic diagram of the front-end (FEM) and back-end (BEM) modules of the TMS. In blue background, we represented the first stage, cooled to 4–10 K, with the FEM. In salmon pink, we represent the BEM modules in the second stage, kept at room temperature.

We present a schematic diagram of the microwave spectrometer for the TMS instrument in Fig. 1. We can divide it into two main stages, depending on the physical temperature at which they are kept. A close cycle helium cooler cools the front-end of the radiometer to 4–10 K, which is the first stage. This front-end includes the optomechanics, the HEMT-based ultra Low Noise Amplifiers (LNA) and a broadband reference load. Two hybrid couplers are used to provide correlation between the two inputs for each polarization. This stage is depicted in Fig. 1 with a blue background. The back-end modules are maintained at room temperature and include room temperature microwave amplifiers, frequency division and definition (depicted in Fig. 1 in salmon pink). A set of downconversion modules and LO distribution blocks provide the down conversion of the subbands to the FPGA baseband. An FPGA-based module that includes ultrafast analog-to-digital conversion performs all the operations related to direct acquisition, processing, formatting and transmission of the data to an application running in a PC.

The design of the microwave radiometer is similar to that of the LFI receivers on-board the Planck mission,[7] which has proven to be particularly robust against $1/f$ gain variations. This robustness is met through a strategy based on pseudo-correlation and a switching of the inputs between a reference signal and the signal of interest on the sky. Both signals travel the same optical path and get switched at the required speed so as not to be affected by the gain variations in the detectors, amplifiers and other drifts due to component imperfections. In the TMS design, this switching scheme has been surpassed by a digital acquisition using high speed ADCs and FPGAs. The receiver in this scheme is not susceptible to gain drifts once the signal has been digitized and will be explained in depth in the following sections. Fig 2 shows the frontend and backend stages of the spectrometer. It can be seen that two orthogonal linear polarizations are coupled from each of a pair of corrugated conical feedhorns. One of the feedhorns looks out of the cryostat at the sky, through a window made of a transparent material to microwave frequencies. The other horn is terminated by a cold calibrator that emits as a blackbody in the operational band to provide a reference signal. Both the sky and reference horn are followed by novel broadband OrthoMode Transducers (OMTs) to couple the aforementioned linear polarizations. The polar signals are fed to

the almost identical arms of the correlator where they are subject to low noise amplification and filtering. The 90° hybrid coupler, which is part of the correlation strategy, is digitally implemented in the FPGA module, which means that the band has to be divided into subbands of ≤ 2.5 GHz that are then downconverted to baseband.

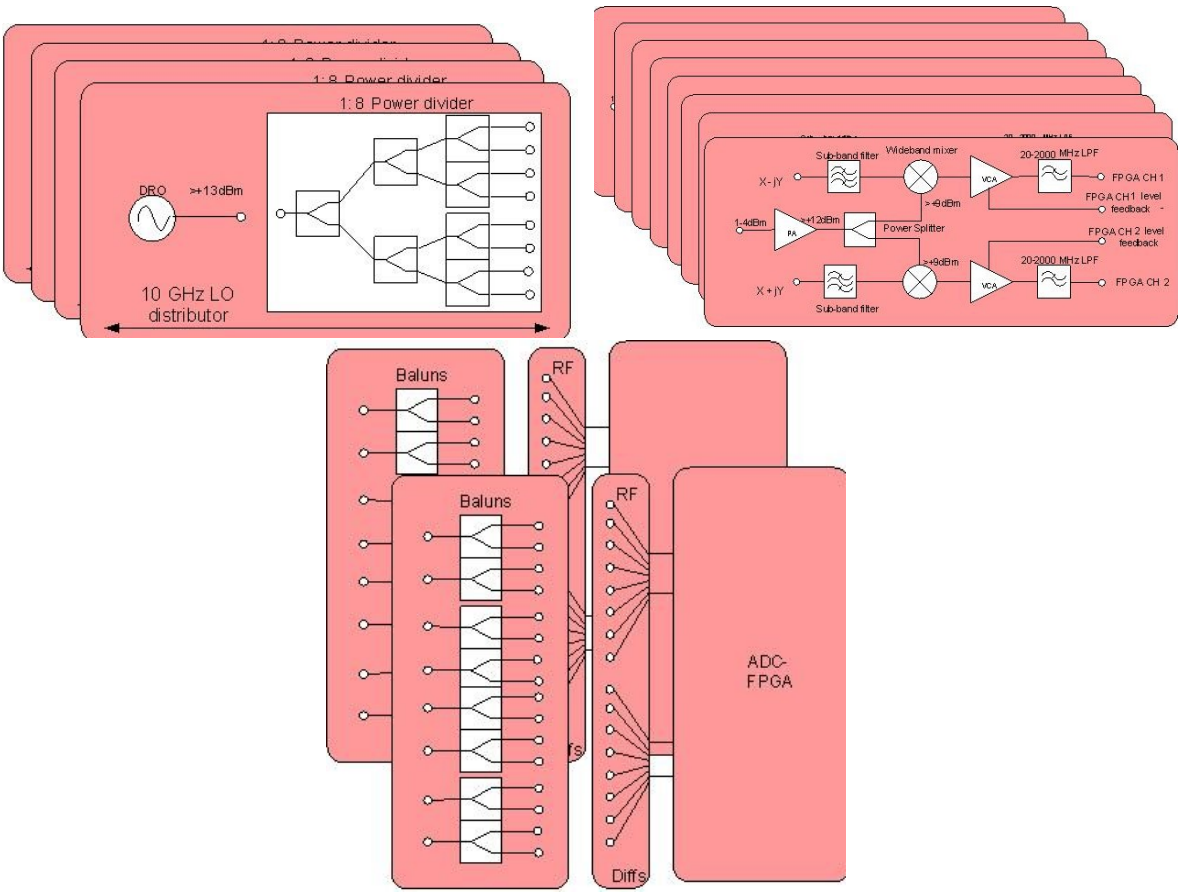

Figure 3: Schematic diagram of the downconverter and FPGA of the TMS. *Up:* the LO distribution blocks and the downconversion modules. *Down:* the ADC-FPGAs.

Figure 2 shows how each of the correlator outputs is fed through a four way diplexer, each corresponding to a different 2 GHz subband in the operational band. The heterodyne scheme is shown in Fig. 3, which interfaces with the acquisition and digitizing process in the FPGA module. The FPGA acquires samples from the four channels, one per subband, at 5.0 Gsps and implements a polyphase filter to reconstruct the spectral distribution of the input signals. As it was mentioned above, after the averaging and Fast Fourier Transform (FFT) operations, this module digitally implements the response of some of the microwave components in order to retrieve the separated sky and reference signals. In addition, the FPGA and downconverter modules contain a gain control unit for optimum ADC performance, and control a fast output to an external PC memory where the data is stored for offline postprocessing.

3. THE TMS CRYOSTAT

The radiometer is required to be cooled inside a cryostat by means of a closed cycle at 4–10 K to ensure the desired sensitivity. Figure 4 shows a detailed view of the already assembled cryostat. The cryostat consists of an axis-symmetric vacuum chamber made of AA6061-T6 with internal dimensions of 970 mm in length and 490 mm in diameter. In order to reach the cryogenic conditions inside it, the instrument is equipped with an air-cooled Pfeiffer ATH-500M turbomolecular pump and a Sumitomo RDK-415D cold head. Final pressure, of the order of 10^{-7} mbar, and the low leak rate the cryostat shows in blind configuration, of the order of 10^{-9} mbar $\cdot$ l/s, maintain nominal temperatures at 50 K and 4 K, respectively.

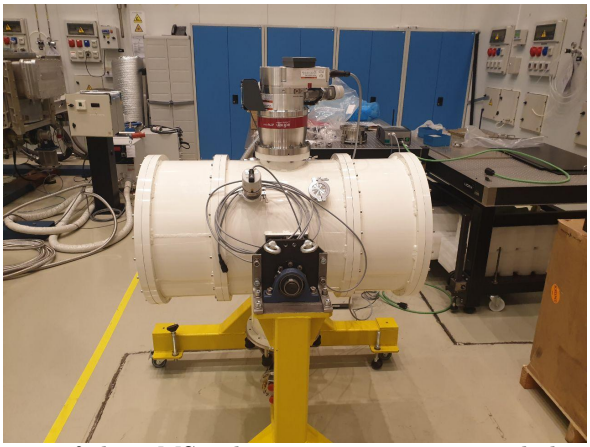

Figure 4: The cryostat subsystem of the TMS. The tests on pumping and thermal performance have already started at the IAC facilities.

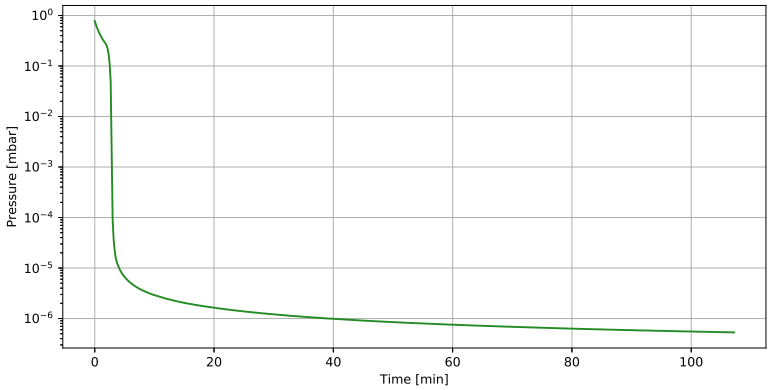

Figure 5: Pumping performance of the TMS cryostat. An ultimate pressure of $5{\cdot}10^{-7}$ mbar is reached after aprox. 100 min.

Figure 5 shows the performance of the cryostat during the pumping. An ultimate pressure of $5{\cdot}10^{-7}$ mbar is reached before starting to cool down.

4. OPTICS

4.1 Feedhorns

Two identical feedhorns have been designed and manufactured to meet strict requirements over the operational bandwidth. In particular, we stipulated that they must provide cross polarization and return loss levels below -35 dB and -25 dB, respectively. We achieved this high performance over the operating bandwidth, between 10–20 GHz, with a novel meta-horn design. For a more comprehensive insight, we direct the readers to the publications[8,9] dedicated to fully describe the design and manufacturing process of these meta-horns. The feedhorns are manufactured in the mechanical workshop as a set of aluminium rings (platelets technique). The rings are stacked to form the meta-surface that was obtained using the design theory followed by optimization with CST Studio Suite. Practical mechanical limitations were also taken into account. The final mechanical horn is shown in Fig. 6.

The antennae radiation patterns are being measured in the far field (FF) regime in the anechoic chamber of the μlab at the University of Milano. Each manufactured feedhorn is to be characterized within the 10–20 GHz range on four copolar and two crosspolar planes, including the copolar E-plane, H-plane and $\pm45^{\circ}$ plane, and the crosspolar $\pm45^{\circ}$ plane. Hereafter, we report the simulation results obtained with CST Studio and SRSR simulation tools, including the radiation patterns at minimum (10 GHz), central (15 GHz) and maximum

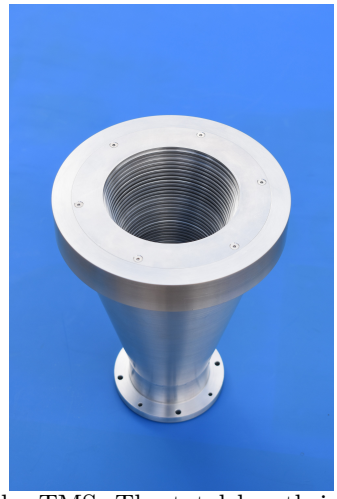

Figure 6: Manufactured meta-horn for the TMS. The total length is 24 cm, the feedhorn aperture presents a diameter of 10.3 cm, with an external diameter of 18 cm, and a 20 mm-diameter feedhorn mouth.

Table 1: Variation with frequency of the metahorn main beam characteristics in the operational bandwidth (10–20 GHz), as simulated by CST software.

Frequency (GHz)	G (dB)	FWHM$_x$ (arcmin)	FWHM$_y$ (arcmin)	e (%)	XPol/CPol (dB)
10	18.6	1352.1	1330.2	1.64	−48.58
12	20.1	1138.8	1145.7	1.22	−54.21
14	21.3	959.5	974.1	1.52	−46.45
16	22.5	826.5	852.4	3.14	−33.83
18	23.3	762.9	803.6	5.33	−33.49
20	22.5	758.6	730.5	3.81	−32.80

(20 GHz) operational frequencies, in Fig. 7, and the simulation for the return loss (S_{11}) in Fig. 8. Table 1 summarizes the main beam properties of the metahorn and their variation with frequency.

4.2 Parabolic Reflector

The configuration of the optical system of the TMS is based on a single, offset-fed reflector, which shall be sub-illuminated by the feedhorn facing the vacuum window. It is designed to provide a stable beam with ∼4° beamwidth and minimal ellipticity over the whole operational bandwidth, as well as low side lobe and cross-polarization levels. The synthesis of the mirror has been planned considering the radiation performance of the feedhorns and the maximum dimensions imposed by the whole system. The mirror is obtained as the circular cross-section of a paraboloid with f/D ratio of 0.77 at an offset angle of 47.7°, resulting in axis lengths of 714.52 and 791.76 mm. The focus of the parabola is coincident with the equivalent phase center of the TMS horn at approximately 15 GHz. The feed is pointed slightly below the center of the reflector, with an angle of 41.24°. This configuration allows edge taper of −20 dB at the edges of the reflector.

Below, we present some preliminary results from the CST simulation of the optical system, for which we have used the Integral Equation Solver. The full wave simulation has been performed for the whole band, between 10–20 GHz, to completely characterize the radiated beam and its variation in the TMS bandwidth. Some relevant radiation characteristics are reported in Table 2. The beam directivity presents a total change of 10% across the band, while the ellipticity is kept under 5% in the first half band, and slightly deteriorated at 19 GHz, with a maximum of 11%. The cross-polar discrimination factor (XPD) is at least 40 dB between 10.5–20 GHz, and reach 32 dB in the lower limit of frequency operation. In addition, Fig. 9 and Fig. 10 show the radiation pattern variation with polarization, based on the comparison of the main figures of merit and beam shape, for two orthogonal polarizations, that is, 0° and 90° linear polarization. Closer inspection shows no significant differences between both polarized fields, with the exception of ellipticity.

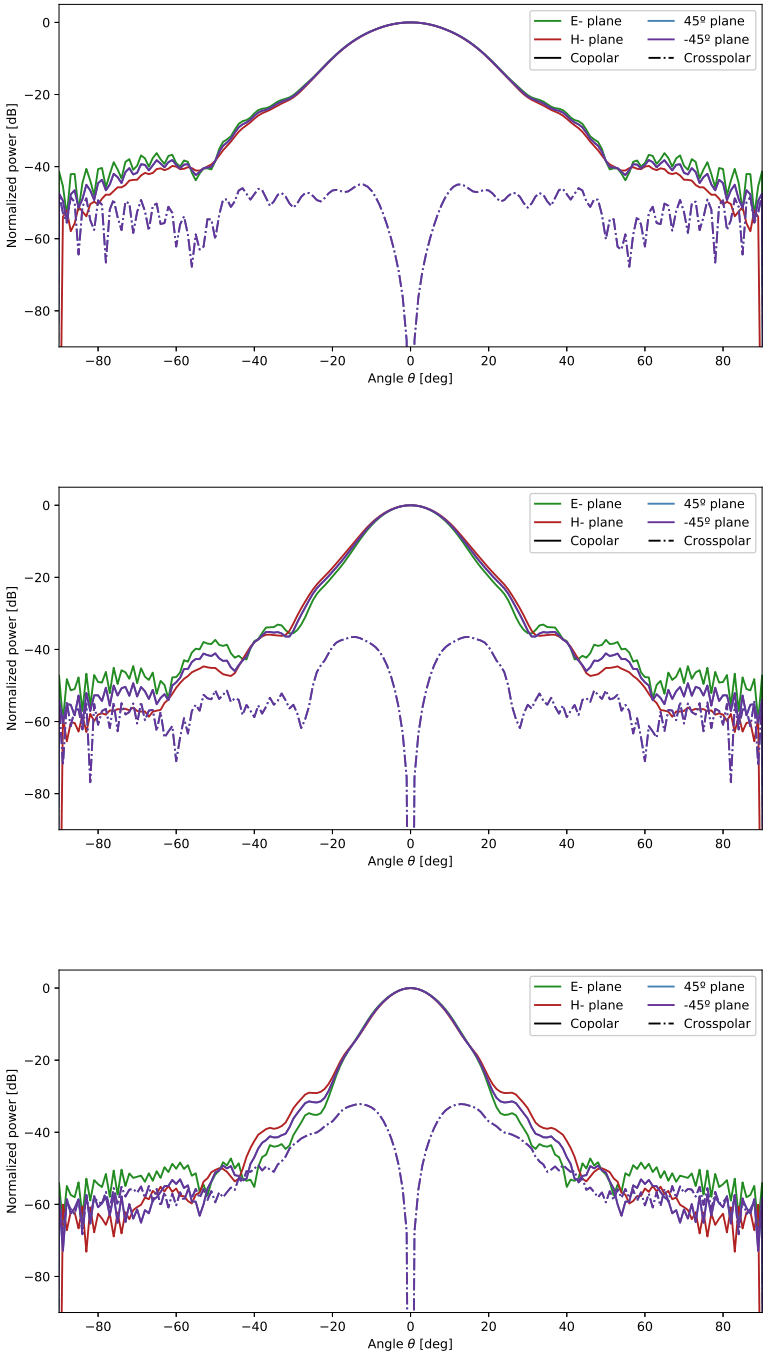

Figure 7: Radiation patterns simulated on CST (confirmed with HFFS and SRSR) simulation software for the TMS "meta-horn" antenna, in the bandwidth between 10–20 GHz. *From top to bottom:* Radiation patterns simulated at 10, 15 and 20 GHz. Copolar planes, including copolar E-, H- and ±45° planes, are represented in solid lines colored in green and red, blue, violet, respectively. Crosspolar ±45° planes are represented with dashed lines, in the same coloring as their copolar counterparts, that is, blue and violet.

The mirror is to be manufactured at the mechanical workshop of the Instituto de Astrofísica de Canarias

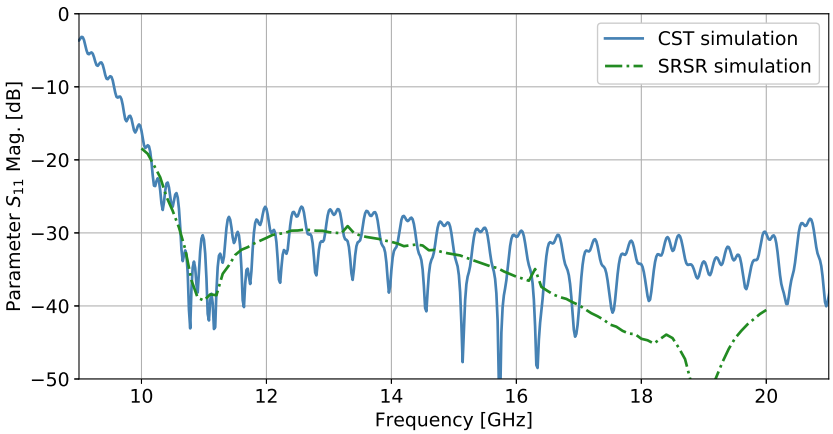

Figure 8: Return loss (S_{11}) of the horn in the operative frequency band. Solid lines in blue and green represent the return losses obtained in the simulations with CST and SRSR software, respectively.

Table 2: Variation with frequency of the main beam characteristics in the operational bandwidth (10–20 GHz), for the 0° polarization.

Frequency (GHz)	Edge Taper (dB)	D_{feed} (dBi)	D_{refl} (dBi)	FWHM (arcmin)	e (%)	XPol/CPol (dB)	η_{spo}
10.0	−15.31	18.63	33.57	197.41	0.96	−32.75	0.947
12.0	−19.65	20.06	36.14	174.26	0.02	−57.46	0.972
14.0	−22.68	21.33	38.62	162.03	1.29	−49.63	0.987
16.0	−29.98	22.46	37.25	153.95	4.04	−44.53	0.993
18.0	−32.33	23.32	37.53	149.78	6.07	−44.16	0.992
20.0	−35.09	23.54	36.96	148.81	8.04	−40.68	0.998

from a single piece of aluminium. The convex side of the mirror shall present a honeycomb structure to lighten the system, while the reflective surface will be polished with a tolerance of $\pm 50\,\mu$m.

5. THE MICROWAVE RECEIVER OF THE TMS

5.1 Internal Calibrator

The pseudo-correlation scheme of the TMS radiometer requires the use of an internal source to generate a reference signal for continuous comparison with the sky emission received through one of the feedhorns. This subsystem shall emit as a quasi-perfect blackbody in the microwave frequencies range, at a physical temperature between 4–10 K in order to be comparable to the sky temperature brightness. Minimizing the imbalance between sky and reference temperatures is a critical instrument requirement, although some authors[10] demonstrate that a proper gain modulation factor can make the sensitivity independent from the reference signal level with the caveat of a small 1/f noise. In addition, to ensure a behaviour as similar as possible to that of an ideal blackbody, requirements for emissivity and temperature homogeneity are extremely demanding.

The design and modelling of a blackbody calibrator can be challenging, as the overall performance results from the convolution of radiometric and thermal performances. In order to ensure both a high emissivity and good thermal conductivity, which are typically incompatible properties, we use a combination of absorbing and metallic materials, and a specially chosen geometry that provides a strong absorption and prevents thermal dishomogeneity.

The TMS 4 K load is being developed by INAF-OAS Bologna.[11] The final design of the 4 K load consists of an array of square-based metal Aluminium pyramids coated with CR/MF 117 Eccosorb material,[12] enhancing the emissivity and temperature homogeneity of the calibrator. The final design is shown in Fig. 11, including a partial representation of the array configuration and a complete $3D$ model including the final shield and clamps to fix it to the feedhorn and thermally decouple it. The optimized dimensions of the pyramids, including the

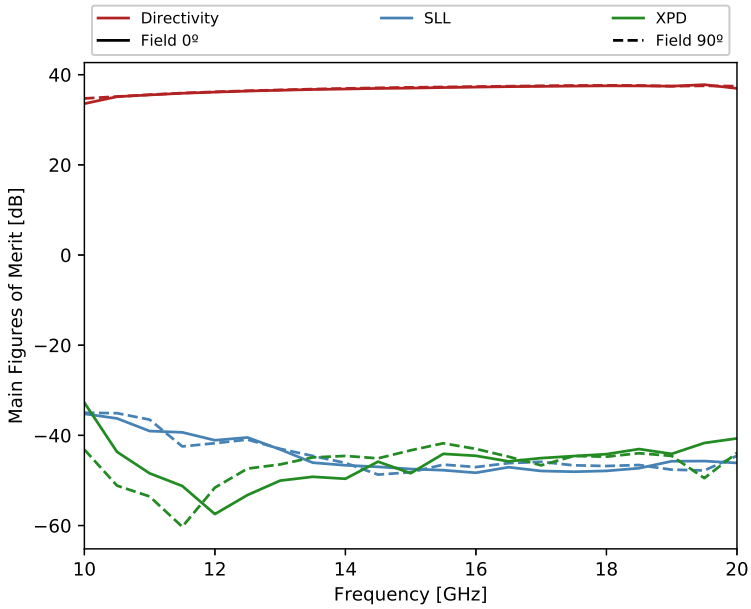

Figure 9: Figures of merit of the radiation pattern for a field excitation with 0° and 90° linear polarization (solid and dashed lines, respectively), and its variation over the operational band of the TMS. We include the directivity and levels for Sidelobes (SLL) and cross-polarization (XPD) in red, blue and green colors, respectively.

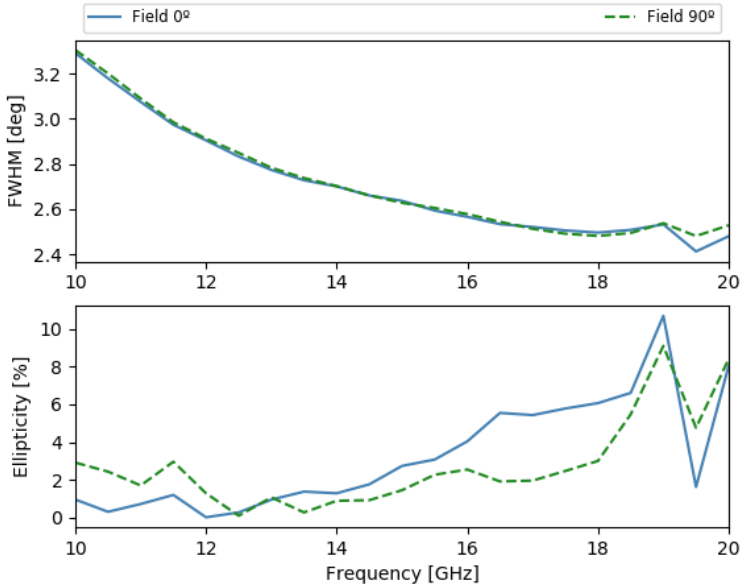

Figure 10: Shape of the main beam for a field excitation with 0° and 90° linear polarization, and its variation over the operational band of the TMS. *Up*: 3 dB beamwidth variation [deg]. *Down*: ellipticity percentage variation. A clear trend with wavelength can be seen.

metal core and absorber coating are $W = 10\,\text{mm}$ and $H = 61\,\text{mm}$. We opted for a final array configuration inside the metal shield with a diameter of 140 mm, a maximum of 14 pyramids, to be consistent with the Near Field (NF) footprints of the TMS feedhorns and provide full coverage along the diameter while keeping size and weight to a minimum to enhance the thermal performance.

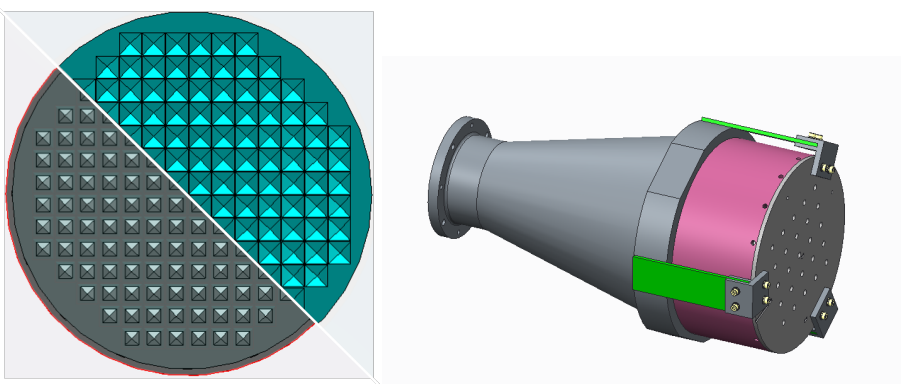

Figure 11: Final design of the internal 4 K load for the TMS. *Left:* Final array configuration, including views from the metal core and the coating layer. *Right:* 3D model of the load-feedhorn system. The load is coupled to the feedhorn by means of three clamps and G10 legs, in green color. The shield is represented in pink and the metal backplate backing the absorber, in grey.

The combined choice of geometry and material results in a device that meets the specified RF and thermal requirements. A thermal model of the load has been developed in ESATAN-TMS software and we have performed a variety of simulations in order to verify if the final design meets the requirements in terms of thermal gradients and stability. Regarding the RF properties, we include the results obtained with the CST Studio Suite analysis software in Fig. 12, which show that the load reflectivity remains below $-40\,\text{dB}$ along the whole observable band. We compare the behaviour of the isolated calibrator, and the combined behaviour of the feedhorn-load system to illustrate the effect of the horn return losses, and how these dominate over the load emissivity. Still, the combination of both components meets the total emissivity requirement set for our scientific goals.

The manufacturing was entrusted to the PMS company in Florence.[13] The load shall soon be ready for its complete characterization in terms of RF properties and thermal performance. This characterization shall include measurements in both room temperature and cryogenic conditions. Figure 13 shows the manufactured calibrator for the TMS instrument.

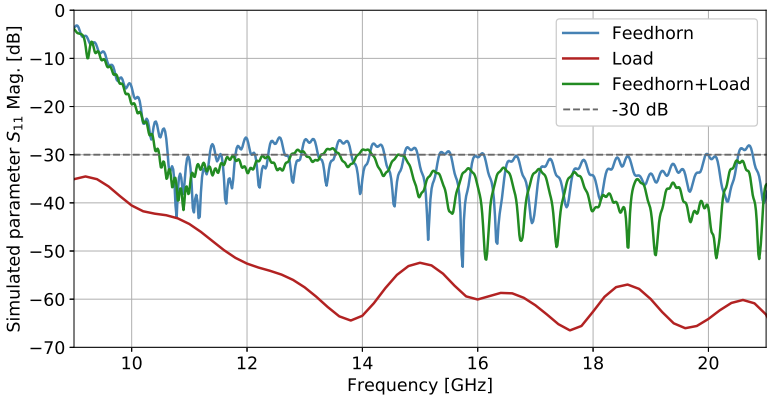

Figure 12: Simulated return loss (S_{11}) of the load-horn system over the operational bandwidth. Return losses never exceed a level of $-40\,\text{dB}$ for the calibration load. Total emissivity is largely dominated by the feedhorn return losses, remaining at a value of $-30\,\text{dB}$.

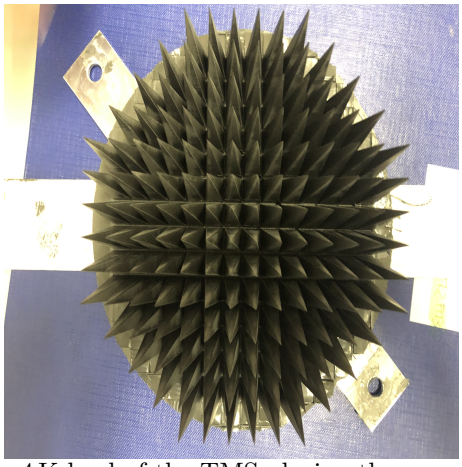

Figure 13: The absorbing part of the 4 K load of the TMS, during the manufacturing at PMS, just after baking and extraction from the mould. The load will undergo a full RF and thermal verification campaign at INAF-OAS Bologna.

5.2 Downconversion Modules

The downconvertion unit consists of two key blocks, namely the mixer unit and the Local Oscillator (LO) distribution unit. The mixer unit is standard for each subband (the input filter will be absorbed into the BEM diplexer) and three inputs; the two corresponding BEM subband outputs and the corresponding LO input.

The mixers are a standard wideband design so these units are generic. The output of each mixer follows an identical path with equal phase. A LNA followed by a low pass filter and gain controlled amplifier make up the signal path. The outputs are fed into the FPGA coaxial interface. A voltage control signal returns the present gain need from the FPGA to maintain the signal at an optimum level for the 12 bit ADCs. The LO input goes into a power amplifier that precedes the mixer. The amplifiers and gain control unit are powered through a common power supply for all the downconversion units. The LO distribution unit consists of a dielectric oscillator (DRO) and a power splitting arrangement to provide 8 outputs of each LO. The units are similar in build with the only difference being the frequency of the DROs (10, 12.5, 15 and 17.5 GHz). The DRO power is supplied from a common unit for all the DRO units. The downconverter, BEM, LO distributor and the FPGA coaxial interface are all connected through semirigid RF coaxial cables to ensure no interference between them whilst also providing a solid RF link. The arrangement has been optimised to minimized costs and many of the units are either designed and built in-house or made up from SMD or drop-in microstrip components.

The FPGA coaxial interface box consists of a set of identical wideband baluns whose input and output are 50 Ω SMA-type connectors. This is needed due to the interface board to the FPGA being balanced output.

6. ELECTRONICS

6.1 The FPGA-based Readout System

We propose a design of a data acquisition system (DAS) based on a System-on-Chip Field Programmable Gate Array (SoC-FPGA) to provide the required capability to digitize and decompose the spectral band between 10–20 GHz, while filtering and correcting radio-interference signals. The intention is to take advantage of the new Xilinx ZCU208 Ultrascale, which presents up to eight 2.5 GHz input channels. The proposed system shall achieve high resolution, fast acquisition, real time signal processing and control, and it is reconfigurable to allow several modes of operation. In addition, it eliminates the troublesome 1/f gain variations of the detectors used in similar instruments, and therefore the need of a fast switching mechanism between the measured signals. The FPGA operation is graphically described in Fig. 14. For the sake of simplicity, the scheme includes the acquisition and processing of one single RF input channel, since all other channels receive the same treatment.

The sampling frequency shall be 5.0 Gsps, establishing a maximum bandwidth of 2.5 GHz at each RF input. A complete downconversion module, previously described in Sec. 2, has been designed to divide the TMS operational

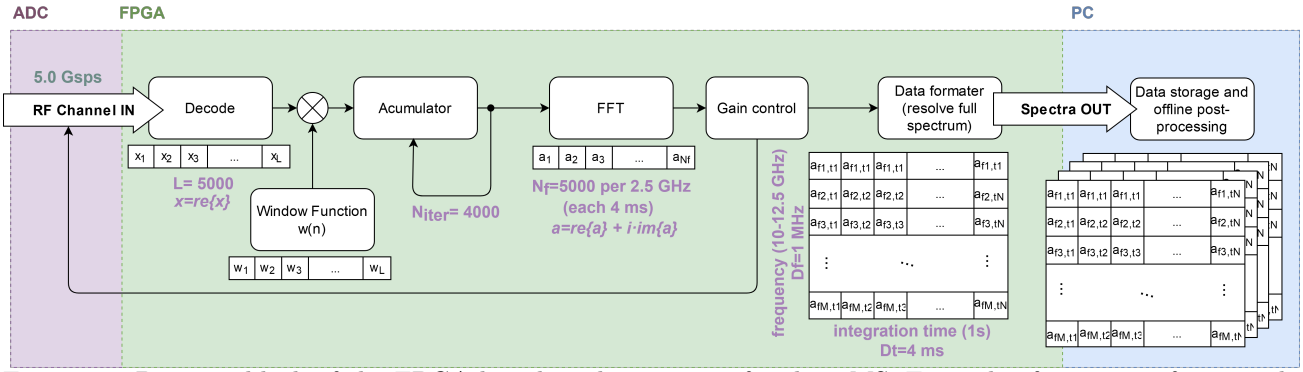

Figure 14: Diagram block of the FPGA-based readout system for the TMS. Example of operation for a single RF channel.

band in the required number of RF inputs. The system has the capability to simultaneously acquire eight RF channels. It presents two modes of operations: in the engineering mode, the system will operate with one, two at most, channels, and will allow to verify the correct behaviour of the SoC; in the science mode, the system will operate continuously performing complete observations. Data will be stored in the internal memory of a PC.

The output rate of the FPGA system, $R_{\rm out}$, is given by the sampling rate of each channel $R_{\rm s}$, the total number of subbands $N_{\rm b}$ and polarizations per band $N_{\rm p}$, the number of bits or quantization levels $N_{\rm q}$, the number of components of the output samples $N_{\rm c}$ (e.g. real/imaginary, magnitude/phase components) and the number of times the measurements are averaged $N_{\rm avg}$, as:

$$R_{\rm out} = \frac{R_{\rm s} \cdot N_{\rm b} \cdot N_{\rm p} \cdot N_{\rm q} \cdot N_{\rm c}}{N_{\rm avg}} \ [\text{bps}]. \tag{1}$$

Table 3 summarizes the values for the design parameters resulting in an output rate of 0.5 Gbps. Currently, two options are being considered: a first, simplified option, in which the FPGA does not operate the Fast Fourier Transform (FFT) of the acquired data and only implements the acquisition and averaging blocks; and a second, more complex option, that performs this operation before transmitting it to the PC unit. In the first case, the number of component outputs $N_{\rm c}$=1, halving the total output rate compared to the second option, in which we have to deal with two output components (real/imaginary). Calculations in Table 3 have been made for the second case.

Table 3: Design parameters and FPGA total output rate.

Parameter	Description	Value	Additional comments	Units
$R_{\rm out}$	Total FPGA output rate	$0.5 \cdot 10^9$	-	bps
$R_{\rm s}$	Sampling rate of each ADC	$5.0 \cdot 10^9$	Maximum sampling frequency of the RF-ADCs of the Zynq UltraScale+ RFSoCs	sps
$N_{\rm b}$	Total number of subbands	4	The total BW is divided in 4 subbands of max. 2.5 GHz to avoid spectral alisasing	
$N_{\rm p}$	Number of polarizations per band	2	A pair of ADCs for each band, X and Y polarizations, making a total of 8 ADCs (max. available)	
$N_{\rm avg}$	Number of times the data are averaged	4000	Configurable	
$N_{\rm q}$	Number of bits for each component	32	Integer, fixed point or floating point	

The data acquired by the system shall be sent to a PC at a transmission rate of no less than 500 Mbps. This communication will be achieved by means of the standard Ethernet protocol using SFP optical interface modules or a RJ-45 interface module.

6.2 Control and Data Storage

An external PC, connected to the FPGA via 10 Gbps fibre optic Ethernet and operating with a real-time application, receives the data and translates them into the load/sky spectral format in order to visualize on the

screen in real time. In addition, the data are stored in an efficient format on a on-board 10 TB hard disk. The PC interface is used for the initial configuration, including the programming of the FPGA, data display and data storage.

The PC, furthermore, is in charge of sending the commands to start and stop the acquisition and the few data required to setup the acquisition. This computer also receives a synchronous time stamp so that the data can be later synchronized with the telescope.

6.3 Signal Processing

In a preliminary design concept, data are stored without further processing, with the exception of the temporal windowing and averaging, previously seen in Fig. 14. Each stored data set contains an averaged complex representation of the linear combination of load and sky signals for a defined polarization. The offline operations block shall include the digital implementation of a hybrid coupler, to decouple both sky and load signals and perform the substraction. This decorrelation operation completes the scheme of the pseudo-correlation architecture described in Sec. 2. Furthermore, and even if it was not the primary goal, the TMS instrument will have polarimetric capabilities, and Stokes parameters can be then calculated with the well-known expressions:

$$\begin{aligned} I &= |E_x|^2 + |E_y|^2, \\ Q &= |E_x|^2 - |E_y|^2 \text{ and} \\ U &= 2 \cdot \Re\{E_x \cdot E_y^*\}, \end{aligned} \tag{2}$$

where all the correlation products are directly obtained from the decoupled output signals.

In addition, we plan to perform the following operations offline: averaging of the data to provide an average level per 1 GHz band; extraction of spectral information about water vapour, ozone and the Galactic emission; and filtering of the unwanted data points due to large interference signals by scanning the power at each frequency point.

7. STATUS, REMAINING WORK AND TIMELINE

We now present the status of the Tenerife Microwave Spectrometer being developed at the Instituto de Astrofísica de Canarias (IAC). We begin describing the current activities regarding the design and development of the TMS. These activities include both design, manufacturing and testing tasks, and a variety of collaborative relationships between our group at the IAC and other international research teams. We conclude this section with a brief description of the next steps and foreseen date for the TMS first light.

Currently, the 4 K Cold Load is in the last stages of the manufacturing process by PMS, Italy. The measurement and testing activities are due in early 2021, including the RF performance in both room and cryogenic temperatures, and also the thermal stability inside the TMS cryostat. We plan also to complete the study and characterisation of the load by means of an equivalent emissivity model, which can help in the instrument calibration in the future.

In a similar way, the design for the TMS reflector will be sent to the mechanical workshop at the IAC for its manufacturing using standard NC milling machines. Regarding the metahorns of the TMS, they have been characterized in the μ-lab of the Università di Milano for their characterisation in terms of their radiation properties, with special emphasis on their cross-polarization levels and wideband performance. Measurement and CST simulations show a very good agreement at the level of fractions of a dB down to the level of the first sidelobes. We can rely on the CST simulations to provide a complete optical characterization of the reflector illuminated by the feedhorn

The cryostat has already been manufactured and sent to the IAC facilities for its testing. Several simulations have been performed to account for its thermal behaviour based on an approximation for the total mass of the Front End modules of the TMS. The approximation for the cold mass was calculated from the actual weight of the manufactured feedhorns and an estimation for the other microwave components based on the equivalent components designed for the radiometers of the QUIJOTE experiment.[14] In addition, the cryostat window,

traditionally made of mylar in previous QUIJOTE experiments,[15] shall be redesigned in order to use UHMWPE material without any effect on the sky beam.

The two hybrid couplers and OMTs, both critical components in the pseudo-correlation architecture, are still in an early stage of design. The requirements we are pursuing for these components are extremely demanding in terms of return loss (-25 dB), port coupling and phase performance ($\pm 3°$), over an octave bandwidth. Commercial microwave components do not meet these requirements, which are critical in order to meet with the scientific goals of the project. We are working on designs for both components based on a novel concept using ridge waveguide in order to obtain the desired performance over the whole instrument bandwidth.

The FPGA board has been tested to verify its adequacy for the TMS experiment, with a series of high level simulations of the FPGA tasks and post-processing operations. We have verified that we should be able to obtain averaged spectra from the sky emission with enough resolution to discriminate and compensate for undesired interference signals from communication satellites. We have established a collaboration with the SSEL group at the Technical University of Cartagena (UPCT). They are currently in charge of the coding and programming of the Xilinx ZCU208 that shall perform the data acquisition, time averaging and sending through an Ethernet link to the PC. The downconversion units have been ordered as commercial sub-components that will be mounted onto PCBs in metallic boxes at the IAC. This allows us to optimize our design for space and performance instead of using packaged components that do not always provide the exact required function. Each of the metallic boxes will provide a well defined function e.g. LO distribution, downconversion, etc. The design has been optimized so that each channel is made up of a few boxes each providing a generic function. In this way the design time is reduced since PCB designs are reused in each channel.

We have just presented the current status of the TMS instrument. We expect to install the TMS instrument, supporting elements and dome by mid 2022.

ACKNOWLEDGMENTS

This work has been partially funded by the Spanish Ministry of Science under the projects IACA15-BE-3707, EQC2018-004918-P, and the Severo Ochoa Program SEV-2015-0548. We acknowledge the support of all the technicians, engineers, scientists and administrative staff of the IAC and QUIJOTE experiment.

REFERENCES

[1] Bennett, C. L., Bay, M., Halpern, M., Hinshaw, G., Jackson, C., Jarosik, N., Kogut, A., Limon, M., Meyer, S. S., Page, L., and et al., "Themicrowave anisotropy probemission," *The Astrophysical Journal* **583**, 1–23 (Jan 2003).

[2] Tauber, J. A. e. a., "Planck pre-launch status: The planck mission," *A&A* **520**, A1 (2010).

[3] Fixsen, D. J. et al., "Calibration of the COBE FIRAS Instrument," *Astrophysical Journal* **420**(2), 457–473 (1994).

[4] Zannoni, M. et al., "TRIS I. Absolute Measurements of the Sky Brightness Temperature at 0.6, 0.82 and 2.5 GHz," *Astrophysical Journal* **688**(2), 12–23 (2008).

[5] Singal, J. et al., "The ARCADE 2 Instrument," *Astrophysical Journal* **730**(2), 138–150 (2011).

[6] Rubiño-Martín, J. A. et al., "The Tenerife Microwave Spectrometer (TMS) experiment: Studying the absolute spectrum of the sky emission in the 10-20GHz range," in [*Society of Photo-Optical Instrumentation Engineers (SPIE) Conference Series*], xxx–xxx (Sept. 2020).

[7] Bersanelli, M. et al., "Planck Pre-Launch Status: Design and Description of the Low Frequency Instrument," *Astronomy and Astrophysics* **520**(A4) (2010).

[8] De Miguel Hernández, J. and Hoyland, R., "Fundamentals of horn antennas with low cross-polarization levels for radioastronomy and satellite communications," *Journal of Instrumentation* **14**, R08001–R08001 (08 2019).

[9] De Miguel Hernández, J., Hoyland, R., Sosa-Cabrera, D., Deviaene, S., Fuerte-Rodríguez, P., González-Carretero, E., and Vega, A., "Manufacturing of 3d-metallic electromagnetic metamaterials for feedhorns used in radioastronomy and satellite communications," *Mechanics of Materials* **139**, 103195 (10 2019).

[10] Seiffert, M. et al., "1/f Noise and other Systematic Effects in the Planck-LFI Radiometers," *Astronomy and Astrophysics* **391**(3), 1185–1197 (2002).

[11] "INAF-OAS Bologna." https://www.oas.inaf.it/. (Accessed: 25 November 2020).

[12] Laird Performance materials, "CR117 Eccosorb material." https://www.laird.com/products. (Accessed: 25 November 2020).

[13] "Pasquali Microwave Systems." https://www.pasquali-microwavesystems.com/. (Accessed: 25 November 2020).

[14] Hoyland, R. J. et al., "The status of the QUIJOTE multifrequency instrument," in [*Millimeter, Submillimeter, and Far-Infrared Detectors and Instrumentation for Astronomy VI*], Holland, W. S., ed., **8452**, 935 – 949, International Society for Optics and Photonics, SPIE (2012).

[15] Rubiño-Martín, J. A., Rebolo, R., Aguiar, M., Génova-Santos, R., Gómez-Reñasco, F., Herreros, J. M., Hoyland, R. J., López-Caraballo, C., Santos, A. E. P., de la Rosa, V. S., Vega-Moreno, A., Viera-Curbelo, T., Martínez-Gonzalez, E., Barreiro, R. B., Casas, F. J., Diego, J. M., Fernández-Cobos, R., Herranz, D., López-Caniego, M., Ortiz, D., Vielva, P., Artal, E., Aja, B., Cagigas, J., Cano, J. L., de la Fuente, L., Mediavilla, A., Terán, J. V., Villa, E., Piccirillo, L., Battye, R., Blackhurst, E., Brown, M., Davies, R. D., Davis, R. J., Dickinson, C., Harper, S., Maffei, B., McCulloch, M., Melhuish, S., Pisano, G., Watson, R. A., Hobson, M., Grainge, K., Lasenby, A., Saunders, R., and Scott, P., "The QUIJOTE-CMB experiment: studying the polarisation of the galactic and cosmological microwave emissions," in [*Ground-based and Airborne Telescopes IV*], Stepp, L. M., Gilmozzi, R., and Hall, H. J., eds., **8444**, 987 – 997, International Society for Optics and Photonics, SPIE (2012).